C. DORRER*,✉
E.M. KOSIK**
I.A. WALMSLEY**

Spatio-temporal characterization of the electric field of ultrashort optical pulses using two-dimensional shearing interferometry

The Institute of Optics, University of Rochester, Rochester, NY 14627, USA

ABSTRACT We report the complete spatio-temporal characterization of ultrashort light pulses using a self-referencing device based on shearing interferometry in the space and frequency domains. The apparatus combines spectral phase interferometry for direct electric field reconstruction with a spectrally resolved spatial shearing interferometer. The electric field as a function of one transverse spatial coordinate and time is obtained by means of a direct algebraic phase-reconstruction algorithm. The method has been tested on several common laboratory situations in which space–time coupling is quantified.

PACS 42.65.Re; 07.60.Ly; 42.25.Bs; 42.30.Rx

1 Introduction

The manipulation and characterization of the electric field of ultrashort light pulses holds the promise of new modes of spectroscopy and thus a deeper understanding of the mechanisms of interaction of light and matter on very short timescales and in a wide variety of materials and structures. For example, it is possible to prepare the electric field so that a particular experiment can be performed most efficiently, or the physical properties of a system can be deduced from the modification of the pulsed field as it passes through the system.

A great deal of work has been done on the characterization of the temporal variation of the field from the early days of mode-locked lasers down to the recently accessed two-cycle regime. One of the earliest methods, and one that is still widely used, is to measure the intensity autocorrelation of the pulse. Although this provides an accurate measure of the root-mean-square temporal duration of the pulse, it does not provide a complete characterization of the temporal intensity, and a fortiori of the electric field. More general approaches have been developed in the past decade that can provide the

✉ E-mail: christophe.dorrer@polytechnique.org
*Present address: Bell Laboratories, 101 Crawfords Corner Road, Holmdel, NJ 07733, USA
**Present address: Clarendon Laboratory, University of Oxford, Parks Road, Oxford OX1 3PU, UK, E-mail: walmsley@physics.osc.ac.uk

electric field as a function of time, or equivalently, of the optical frequency [1]. These approaches often have analogs in the spatial domain, and frequently borrow much from their spatial counterparts both in terms of their principle of operation and the inversion algorithms. Nonetheless, their experimental implementation is more complicated because of the difficulty of manipulating the electric field with sufficient temporal resolution. It is often useful to categorize these methods according to their approach to extracting the electric field from the measured data as spectrographic [2–8], interferometric [9–13] and tomographic [14–17]. This is not an exhaustive classification, however, and there are a number of methods that make use of multiple independent data sets to estimate the pulse shape [18–21]. All of these techniques assume that the temporal characteristics of the pulse are independent of the spatial characteristics. When this assumption is not valid, they either reconstruct an average temporal field over the spatial variations or give biased results (as is the case, for instance, for all techniques based on time-to-space encoding to implement single-shot operation). Space–time coupling, i.e. the situation where the temporal field is spatially dependent, is a common situation in ultrafast optics. It is for example a key element in the generation and amplification of ultrashort pulses. It also arises, detrimentally, when manipulating ultrashort optical pulses. For example, the focusing of an ultrashort light pulse [22], its shaping using a zero-dispersion line [23] or its propagation in a misaligned compressor [24] all generate space–time coupling. Such effects are probably significant in a lot of experiments, though they are rarely discussed when the experimental results are not as expected. More importantly, space–time shaping of the electric field is a promising tool for coherent control [25, 26] and non-linear optics [27], and calls for an appropriate diagnostic.

In contrast, measuring the spatial dependence of the field of monochromatic coherent radiation is a much older and more established concept [28, 29]. It encompasses optical testing and wavefront measurement, and includes many techniques for extracting the spatial phase of the electric field. In this paper, we show how to combine a method of characterizing the temporal variation of the field with a method for characterizing the spatial variation, to provide complete spatio-temporal pulse characterization.

We first review the techniques that have been implemented previously to estimate the spatio-temporal field
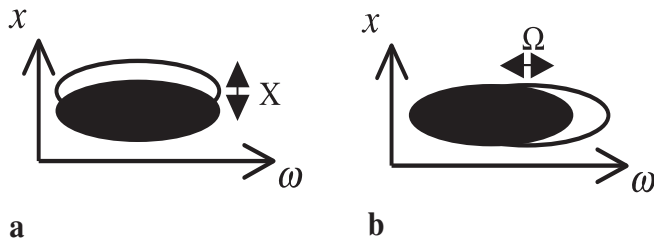
FIGURE 1 Implementation of shearing interferometry in the (x, ω) domain using a shear X in the spatial domain (**a**) and a shear Ω in the spectral domain (**b**)

$E(x, t)$ or equivalently the spatio-spectral field $\widetilde{E}(x, \omega)$ of an ultrashort light pulse. We then present a self-referencing device capable of measuring the electric field $\widetilde{E}(x, \omega)$ as a function of the optical frequency ω and a transverse spatial coordinate x by means of shearing interferometry in these two domains (see Fig. 1). The new method is more generally applicable than previous methods, and has some important practical advantages. The method of spectral phase interferometry for direct electric field reconstruction (SPIDER) [11, 30, 31] is used to generate a spectral shear, while a Michelson interferometer generates a spatial shear. The experimental trace is composed of two interferograms that can be measured simultaneously with a single two-dimensional imaging spectrometer. The electric field is extracted directly and algebraically using standard phase-reconstruction procedures, ensuring accuracy and speed. Several experimental applications of this new tool are presented.

2   Problems and solutions for the spatio-temporal characterization of ultrashort optical pulses

We restrict our attention in this paper to a single spatial variable. Therefore, we consider the analytic signal of the electric field of an ultrashort light pulse $\widetilde{E}(x, \omega)$ as a complex function of the frequency ω and a space variable x. Extension to the two transverse spatial variables would need slight adaptation. For example, it is possible to completely characterize a slice of the electric field $\widetilde{E}(x, y, \omega)$ as a function of x and ω for a given y, and then scan the beam at the input of the measurement device to modify y. The amount of data is obviously much larger. This complete characterization as a function of x, y and ω, although it would be useful in some experimental situations where no symmetry exists for the field, is not mandatory for the experimental cases we present in this article.

The spatio-spectral intensity $I(x, \omega) = \left| \widetilde{E}(x, \omega) \right|^2$ can be obtained using a two-dimensional spectrometer, which measures the spectral density of an optical radiation as a function of the position on the input slit. This is obviously not sufficient to completely characterize the electric field, as it yields no information on the phase $\varphi(x, \omega)$. It is known that a non-stationary filter, most often synthesized using non-linear optics, is necessary to characterize ultrashort pulses. This is of course also the case if one measures the temporal pulse shape as a function of the position in the beam.

Any time-domain method needs to be combined with a method for spatial phase measurement. There are a number of well-known approaches to achieve such a task. A Shack–Hartmann sensor, for example, measures the local slope of the wavefront around a position x within the beam. The slope is obtained by measuring the position of a spot focused by a microlens located at x relative to the location of the optical axis of the microlens. If the light incident on the microlens is broadband, each frequency is focused independently, most likely to a slightly different location in the focal plane of the microlens depending upon the wavefront at that particular frequency. With a single detector, however, no frequency-resolved information about the pulse is obtained. An interferometric technique for the measurement of the wavefront might be similarly difficult because of the dependence of the fringe spacing on the wavelength. An ultrashort pulse generally has a broad spectrum, requiring the use of a carefully designed achromatic interferometer. Once again, no frequency-dependent information can be obtained from such an interferometer. However, if the wavefront is resolved in frequency (for example if one spectrally filters the input pulse before the wavefront measurement device and measures the spatial phase for different optical frequencies), one can extract at best the spatio-spectral phase function $\varphi(x, \omega) + \alpha(\omega)$, where α is an arbitrary function of the optical frequency ω [32]. The determination of this function requires at least the complete characterization of the temporal pulse shape at a reference point in space (if all the frequencies composing the pulse are present at this reference point), but is more involved in the general case.

In contrast, generic pulse-characterization techniques assume that the temporal evolution is identical at every position in the beam. In general, the pulse is not spatially resolved either during the non-linear interaction or the detection. In fact, it is an interesting problem to determine what is measured in the case of a spatially non-uniform pulse. The answer is certainly very dependent upon the particular approach, the way the non-linear interaction is implemented and the acquisition of the experimental trace. Measuring the field as a function of frequency and space thus requires an approach where both frequency and spatial resolution are used.

Among the first approaches to the problem of spatio-temporal pulse characterization was a test-plus-reference method developed by Diddams et al. to study non-linear propagation [33] (and in earlier unpublished work by Fittinghoff). In these methods, a reference field is generated from the input field by means of a spatial filter consisting of a pinhole located at position x_0 in the pulse beam. This is re-collimated using a lens or mirror to approximate a plane wave front, similar to what is done in point-diffraction interferometers [34]. In the ideal case, one obtains a pulse with a phase that is not spatially dependent and has the spectral dependence of the field at x_0, implying that $\varphi_{\text{ref}}(x, \omega) = \varphi(x_0, \omega)$. Spatially resolved Fourier transform spectral interferometry between this reference field and the unknown field yields the spectral phase difference $\varphi(x, \omega) - \varphi(x_0, \omega)$. A supplemental measurement of the spectral phase of the pulse at the reference point, using a standard pulse characterization technique, gives $\varphi(x_0, \omega)$, which means that one can easily obtain the spatio-spectral phase of the input pulse $\varphi(x, \omega)$ by subtraction. However, this will only work if there exists a point in the beam where all optical frequencies contained in the pulse

are present. In most situations of interest this is not the case, for example, in the presence of spatial chirp. It also relies on the ability to perfectly collimate a point source into a plane wave, which for ultrabroadband pulses is technically difficult to achieve without space–time coupling. Furthermore, the principle of the measurement makes single-shot operation difficult (in the particular case mentioned, one two-dimensional spectrometer is needed to perform the spectral interferometry measurement, and a second would be needed if one wanted to use single-shot frequency-resolved optical gating to characterize the field at the reference point).

Spectral phase interferometry for direct electric field reconstruction (SPIDER) has the advantage of measuring the spectral phase at a given spatial point using only a one-dimensional interferogram, which can be acquired using a standard non-imaging spectrometer. It can thus be extended to the characterization of the spectral phase of a pulse as a function of position in the beam using an imaging spectrometer and a two-dimensional detector [35]. However, this alone is not capable of providing information on the wavefront of the pulses, even though it reveals interesting signatures of spatio-spectral coupling in the sub-ten-fs pulses generated by a mode-locked laser.

Another approach to obtain information on spatio-temporal coupling is based on an inverted autocorrelator [36]. A beam undergoes lateral spatial inversion by reflection from an odd number of mirrors. The inverted autocorrelator uses this phenomenon in one of its arms, and retains an even number of mirrors in the other arm. This makes such a device sensitive to spatial chirp, or more particularly the variation of the group delay with lateral position in the beam. This sensitivity allows one to adjust the parallelism of the gratings of the compressor in a chirped-pulse amplification system, as well as the distance between the two gratings. Again, it does not provide complete characterization of the pulse but is limited to the quantification of spatial chirp.

Another example of the importance of spatio-temporal beam characterization is the measurement of the response function $R(x, \omega)$ of a linear optical system as a function of space and frequency [37]. This follows the familiar pattern of a test-plus-reference interferometer with both spatial and spectral resolution of the output field. Specifically, a fraction of an unknown input field is sent to the optical system whose response is to be determined, while the rest is kept as a reference that bypasses the system. The two fields are interfered and the fringe pattern detected as a function of space and frequency. One can show that the modulation term is equal to $I(x, \omega) R(x, \omega)$, so that the complex response function $R(x, \omega)$ can be extracted. Optical systems tested in this way include simple lens and assemblies of lenses, a prism, a zero-dispersion line or even a complete chirped-pulse amplification system. This is an extension of the measurement of the modulation transfer function of an optical system [38], which has been performed with various interferometric and non-linear techniques [39–42]. These techniques extend optical testing to the space–frequency domain but do not measure the field itself. Of course, if the input field is known, one can completely characterize the output field, but this begs the question of the spatio-temporal characterization of the input field.

3 Two-dimensional shearing interferometry

3.1 Introduction

We demonstrate in this paper a method based on two-dimensional shearing interferometry in the spatio-spectral domain (x, ω). Our instrument directly measures the spatio-spectral phase function $\varphi(x, \omega)$. A complete description of the field $\widetilde{E}(x, \omega)$ is obtained from the phase and an ancillary measurement of the spatio-spectral intensity $I(x, \omega)$. Shearing interferometry is a well-known technique for the measurement of wavefronts in the spatial domain [43]. It functions by interfering the wavefront $\varphi(x, y)$ under test with a replica of itself shifted (laterally sheared) along the x axis by a distance X. At a given spatial point (x, y) on the detector, the phase difference $\varphi(x + X, y) - \varphi(x, y)$ can be extracted from the measured interferogram. If the points are sufficiently close, this phase difference is proportional to the gradient $\dfrac{\partial \varphi}{\partial x}$. Two independent gradients of the phase (most often in orthogonal directions) are obtained from two two-dimensional interferograms with independent lateral shears. These interferograms contain redundant information, so that it is possible to obtain an optimal fit (in the least-square sense) to the two-dimensional spatial phase.

SPIDER is essentially one-dimensional shearing interferometry in the optical frequency domain. Its implementation is more complicated than for its spatial counterpart because it requires non-linear optics to generate a spectral shear. It has the important feature, however, that it can be extended to allow the reconstruction of the spatio-spectral phase from a measurement of the spatial and spectral gradients of the phase, i.e. $\dfrac{\partial \varphi}{\partial \omega}(x, \omega)$ and $\dfrac{\partial \varphi}{\partial x}(x, \omega)$. To do this, one must design an apparatus that can generate both a spatial shear X and a spectral shear Ω (Fig. 1). The apparatus and procedures needed for this task are described in the next two sections.

3.2 Generation of a spectral shear

In conventional SPIDER, the non-linear interaction of two replicas of the pulse with the instantaneous frequencies ω_0 and $\omega_0 + \Omega$ of a highly chirped pulse results in two converted pulses relatively sheared by Ω and delayed by τ (assuming that there is no spatial dependence of the temporal pulse shape of the test electric field pulse). From the resulting one-dimensional interferogram, it is straightforward to extract the spectral gradient $\dfrac{\partial \varphi}{\partial \omega}$ of the phase φ of the input pulse, which can be integrated to retrieve φ. This principle can be extended to spatially resolve the spectral phase gradient if the spatial information is preserved during the non-linear interaction and the acquisition of the interferogram.

Figure 2a illustrates the technique we have experimentally used to obtain the results presented in this paper. Two replicas of the input pulse, separated by a time delay τ are generated using a Michelson interferometer. The non-linear interaction between these two replicas and the chirped pulse takes place at the Fourier plane of a double-Fourier-transform set-up. In this arrangement, the first lens focuses the two replicas in the non-linear crystal, where they interact with
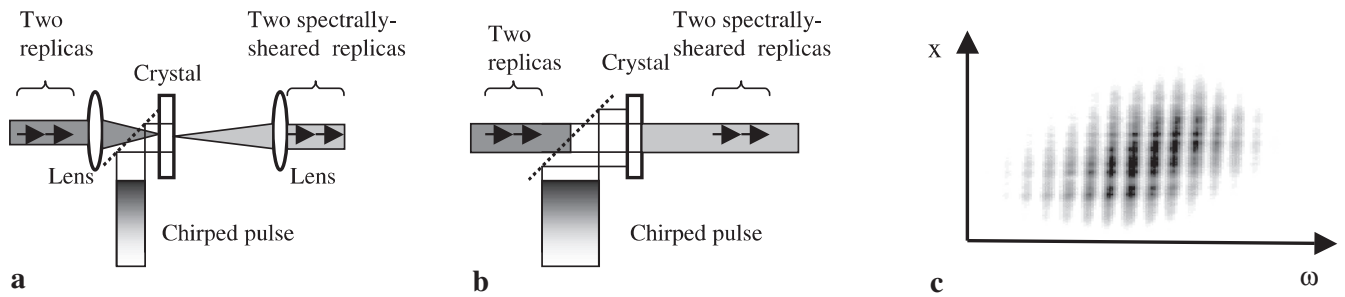
FIGURE 2 Generation of a spectral shear. In **a**, the non-linear interaction is performed with two focused replicas of the input field and an unfocused chirped pulse. In **b**, the non-linear interaction is performed with two unfocused replicas of the input field and a spatially expanded chirped pulse. In the resulting experimental interferogram, plotted in **c**, the fringes are due to the delay τ between the two interfering pulses, so that they are perpendicular to the frequency axis. This measurement was performed around the upconverted frequency

an unfocused chirped pulse. The up-converted replicas are recombined by the second lens. The set-up ensures that the two replicas experience locally a spatially flat phase and intensity that is also quasi-monochromatic. It has the drawback, however, that it is necessary to manipulate the test pulse replicas, which can be difficult if their bandwidth is very large. We did not encounter this problem in our case, where the total bandwidth of the pulses was of the order of 40 nm.

Another possibility, sketched in Fig. 2b, is to spatially filter the chirped pulse with a pinhole and recollimate it in order to obtain quasi-plane waves at frequencies ω_0 and $\omega_0 + \Omega$ (the requirement is far less stringent than for the technique described in [33], since one recollimates two very close frequencies, and not a broadband pulse). Two unfocused replicas of the input pulse can be up-converted with this chirped wave in the non-linear crystal, with the advantage that no focusing or other manipulation of the replicas of the test pulse is needed. An alternate method to obtain plane waves at the two frequencies used for upconversion is to expand the chirped beam. Note that it is important that one has energy at frequencies ω_0 and $\omega_0 + \Omega$ for all values of x where the two replicas have non-zero intensity. However, the spatial variation of the intensity does not compromise the accuracy, since the phase information is encoded in the rapidly varying fringe pattern. If the wavefront at these two frequencies is not flat, a frequency-independent spatial phase will be added to the retrieved spectral gradient. The reconstructed pulse shape at each point is thus not affected, but the time delay with respect to a common temporal origin is lost. Nevertheless, one can show that it is possible to faithfully reconstruct the full phase profile $\varphi(x, \omega)$ since the missing information is contained in the spatial gradient.

All these configurations generate two replicas of the input field $\widetilde{E}(x, \omega - \omega_0)$ and $\widetilde{E}(x, \omega - \omega_0 - \Omega)$. The resulting interferogram was measured as a function of x and ω with a two-dimensional imaging spectrometer, as illustrated in Fig. 2c. Fringes due to the delay τ are clearly visible. By applying the common filtering operation of conventional Fourier transform spectral interferometry to each spatial line of the interferogram, one obtains the spectral gradient $\dfrac{\partial \varphi}{\partial \omega}(x, \omega)$. This information gives the pulse shape at each location in the beam, but contains no wavefront information (for example, it is not sensitive to the focusing of the test pulses) [35].

SPIDER is ideally suited for the measurement of this spatially resolved spectral phase gradient since it only needs a one-dimensional interferogram to characterize the pulse shape at a given point, so that extension to a line in the beam using a two-dimensional spectrometer is straightforward. Most other techniques need a two-dimensional spectrometer to measure the pulse shape at a single spatial point, and so cannot be generalized. As the direct inversion algorithm of SPIDER takes only a few milliseconds to retrieve the pulse shape, the processing of the two-dimensional interferogram is done in less than a second, which is comparable to the time it takes other techniques to retrieve the pulse shape at one point in the beam using iterative deconvolution algorithms.

3.3   *Generation of a spatial shear*

The spatial gradient $\dfrac{\partial \varphi}{\partial x}(x, \omega)$ is measured by imaging the beam at the fundamental frequency on the slit of the imaging spectrometer after passing it through a Michelson interferometer (see Fig. 3a). The interferometer provides independent control of the shear, tilt and delay between the two imaged pulses. For a given tilt K, shear X and delay T, the detected signal on a two-dimensional array is $|E(x + X, \omega) + E(x, \omega) \exp(iKx) \exp(i\omega T)|^2$, from which $\varphi(x + X, \omega) - \varphi(x, \omega) + Kx + \omega T$ can be extracted by standard Fourier processing if the fringe modulation due to $Kx + \omega T$ is sufficiently large that the cross-correlation terms are separated from the autocorrelation term in the transform domain. In order to observe interference between the two fields, the delay T must be smaller than the time window allowed by the spectrometer resolution. An experimental interferogram measured at the output of such an interferometer is displayed in Fig. 3b. In this particular case, the delay T is equal to zero, and the fringes are only due to the tilt between the two wavefronts.

As in all other implementations of shearing interferometry using a spatial or spectral fringe carrier frequency, a precise calibration of the linear term of the extracted phase gradient must be performed. If this is not done, any component of the phase that remains is linear in the respective variable (ω or x) and is integrated into a systematic quadratic phase. In conventional SPIDER, for example, a precise calibration of the delay between the two test pulses is necessary [44]. In space–time SPIDER, a calibration trace is required in order to
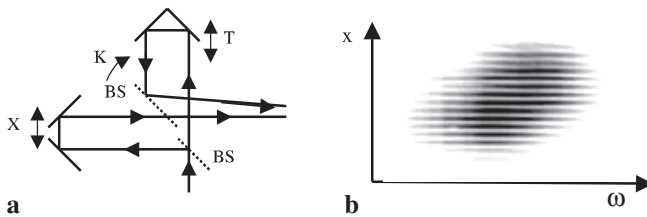
FIGURE 3 a Generation of a spatial shear using a Michelson interferometer with independent setting of the shear X, tilt K and delay T. The shear and delay between the two fields can be adjusted by translating the pair of folding mirrors while the tilt can be adjusted by tilting one of the beam splitters (BS). **b** Experimental interferogram obtained from this interferometer. Note that in the plotted case, the fringes are due to the tilt between the two fields (the delay T is close to zero), so that they are perpendicular to the spatial axis. This measurement was performed around the fundamental frequency

remove the phase $Kx + \omega T$ from the data. This trace can be recorded by nulling the shear, provided this operation can be performed without modifying the tilt and delay between the two replicas. Another precise way of calibrating the device is to double-pass the test pulse pair through the interferometer. This leads to four replicas of the pulse, among which two replicas have zero shear but have a relative phase $2Kx + 2\omega T$. This phase difference can be used as a calibration for all further measurements.

3.4   *Additional comments*

In our experimental demonstration, the two interferograms are measured sequentially. The corresponding gradients are extracted, and then used to reconstruct the phase. If needed, single-shot operation can be implemented for the measurement of the phase, i.e. the two interferograms can be measured simultaneously with the same spectrometer on a single laser shot. Indeed, the spatial and spectral phase gradients are extracted separately because of the different carrier modulation used for each interferogram, so that the fringes of the two interferograms are not parallel (a delay between the two output replicas for the SPIDER spectral shearing interferometer and a tilt between the two replicas for the spatial shearing interferometer lead to orthogonal fringes on the detector). Consequently the components in which the phase gradients are encoded are located at different positions in the two-dimensional Fourier plane.

In our implementation, the spatial gradient is extracted from an interferogram measured at the fundamental optical frequency of the pulse. Alternatively, one could also send a single up-converted replica into the Michelson interferometer, and measure a shearing interferogram at the second harmonic frequency. An advantage of working at the fundamental frequency is that the energy at the detector is much higher for a fixed input energy, which makes the measurement easier to perform. As in [45], one can measure simultaneously and independently an interferogram at the fundamental frequency and an interferogram at the converted frequency using the first and second orders of diffraction of the grating of the spectrometer. Because the two phase gradients can be measured simultaneously by superimposing the spatial and spectral shearing interferograms, a single-shot measurement of the phase of the input field is possible. Various procedures can be used to reconstruct the phase from the two gradients

$\frac{\partial \varphi}{\partial x}(x, \omega)$ and $\frac{\partial \varphi}{\partial \omega}(x, \omega)$. Based on the extensive work done in two-dimensional spatial shearing interferometry, the phase can be reconstructed.

The linear spectrally resolved shearing interferometer is very sensitive. From our implementation, it is estimated that single-shot operation can be obtained with a 200-nJ input-pulse energy. The same signal would be obtained by integrating a 100 MHz train of 2 fJ pulses for 1 s. The spatially resolved SPIDER device, because it relies on a non-linear interaction using a large-area beam, is estimated to yield accurate single-shot operation for a 300-µJ pulse. Although significantly higher than for the spatial shearing interferogram, this energy is nonetheless accessible by many amplified short-pulse laser systems, and could be scaled down somewhat by adapting the geometry of the non-linear interaction and measurement.

## 4   **Experimental results**

This new characterization device has been extensively tested in several experimental configurations that are common in ultrafast optics. In our tests, we used 60-fs pulses from a home-built 1 kHz Ti:Sa chirped-pulse amplification (C.P.A.) system containing about 450 µJ per pulse. The central wavelength was 815 nm. The beam was down-collimated using a two-lens telescope to a beam with a full width at half maximum (FWHM) of 2 mm. The input pulse was split into two pulses, from which one was sent to the spectral shearing interferometer while the other was sent to the spatial shearing interferometer. In the spectral shearing interferometer, the pulse was split into two pulses. One of these pulses was sent to a Michelson interferometer while the other was sent to a two-grating compressor. The Michelson interferometer generated two replicas of the input pulse, separated by a delay of around 2 ps. The compressor generated a chirped pulse with a second-order dispersion equal to 3.48×10^5 fs^2. These parameters allowed one to generate a spectral shear $\Omega = 5.7$ ps^{-1}, i.e. of the order of 10% of the spectral FWHM of our pulse. This quantity was calibrated by measuring the dispersion of the compressor and the delay between the two pulses. The two replicas were recombined with the chirped pulse, and non-linear interaction took place using the geometry of Fig. 2a. The non-linear crystal was a 250-µm-long Type II BBO crystal. When designing the apparatus, it must be kept in mind that a thick crystal could introduce significant space–time coupling in some interaction geometries. This interferometer led to two spectrally sheared, temporally delayed replicas of the input pulse, at a wavelength of around 400 nm. The spatial shearing interferometer closely followed the sketch of Fig. 3a, and generated two spatially sheared replicas of the input pulse around 800 nm. We used a shear of the order of 10% of the spatial FWHM of our beam. This quantity was calibrated by measuring the spatio-spectral intensity of each independent beam by successively blocking each arm of the interferometer. The outputs of the spatial and spectra shearing interferometer were sent to a Triax imaging spectrometer from Jobin Yvon, set to measure light around 800 nm and 400 nm. The focal length of this spectrometer was 30 cm. The 600 gr/mm diffraction grating was blazed at 750 nm, and this ensured

good diffraction efficiency in the first order around 800 nm and in the second order at 400 nm. The slit was opened to 100 μm, which allowed good sensitivity with sufficient spectral resolution. The CCD camera at the Fourier plane of the spectrometer was an IMG camera from Finger Lakes Instruments. Our images were composed of 512 by 512 pixels, with a size of 25 μm by 25 μm. The analog-to-digital converter had a dynamic range of 16 bits. For the results presented in this paper, we independently measured the two interferograms. This allowed one to independently set the integration time for each image in order to maximize the individual signal-to-noise ratio.

The separation of the two lenses of the telescope was changed to modify the wavefront of the beam by inducing a quadratic spatial phase, while changes in the distance between the two gratings of the compressor at the end of the chirped-pulse amplification system were used modify the pulse shape by inducing mainly quadratic spectral phases. Figure 4 shows various spatio-spectral phases obtained by modifying these parameters. All measured modulations agreed well with the modulations calculated using the parameters of the telescope and compressor. It is worth noting that in all these cases the amount of space–time coupling was very small. Indeed, the phase introduced by the compressor was not spatially dependent, and the phase introduced by the telescope was only slightly spectrally dependent.

Diffraction and refraction are well-known sources of space–time coupling, and are widely used in the generation and manipulation of ultrashort optical pulses [46]. Prisms and gratings introduce angular dispersion. Although this dispersion arises from very different mechanisms, it can be described using the usual formalism based on the first-order expansion of the phase as a function of transverse coordinate and frequency. In the (k, ω) domain, the input and output fields are related by $\widetilde{E}_{\text{output}}(k, \omega) = \widetilde{E}_{\text{input}}(k - \gamma\omega, \omega)$, showing a linear dependence of the direction of propagation k upon the frequency ω. The constant of proportionality, γ, is proportional to the angular dispersion introduced by the element considered and can be calculated from its properties (for example, groove spacing and angle of incidence for a grating). This is equivalent to the representations $\widetilde{E}_{\text{output}}(x, \omega) = \widetilde{E}_{\text{input}}(x, \omega) \exp(i\gamma\omega x)$, in the (x, ω) domain or $\widetilde{E}_{\text{output}}(x, t) = \widetilde{E}_{\text{input}}(x, t - \gamma x)$ in the (x, t) domain. In the (x, t) domain, the resulting spatio-temporal dependence is known as pulse-front tilt, and corresponds to the situation where the time of arrival of the energy in a plane perpendicular to the direction of propagation depends upon the position. Angular dispersion and pulse-front tilt are always equivalent because of the Fourier duality between the (k, ω) and (x, t) domains [47].

This coupling can be seen quite strikingly in Fig. 5, which shows a contour plot of the intensity of the pulse in the (x, t) space after it has propagated through a Brewster-cut fused silica prism and an equilateral SF10 prism. The
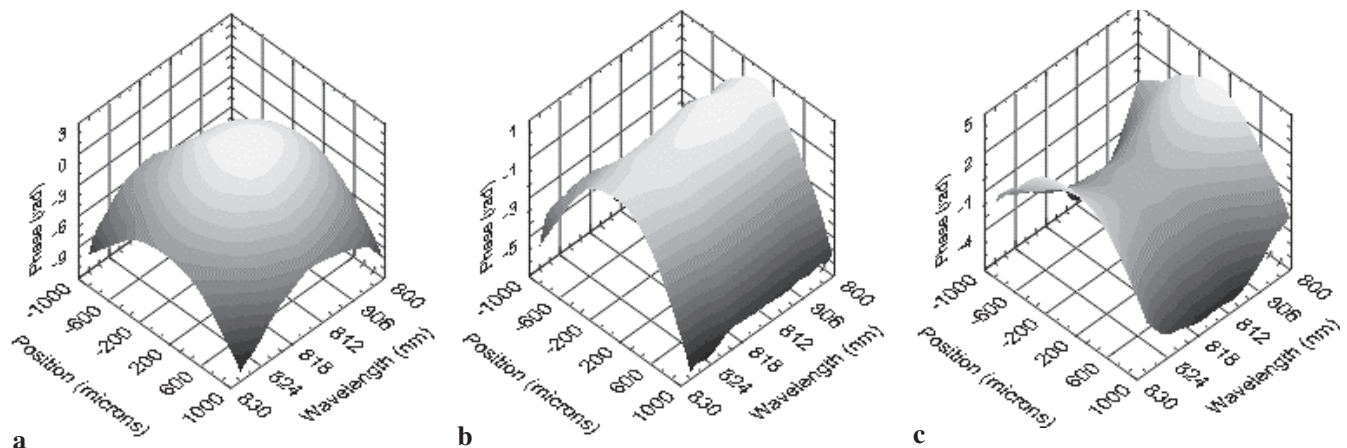
FIGURE 4 Spatio-spectral phase of the electric field for a focusing beam with negative chirp (**a**), close to temporally Fourier transform-limited (**b**) and positive chirp (**c**)
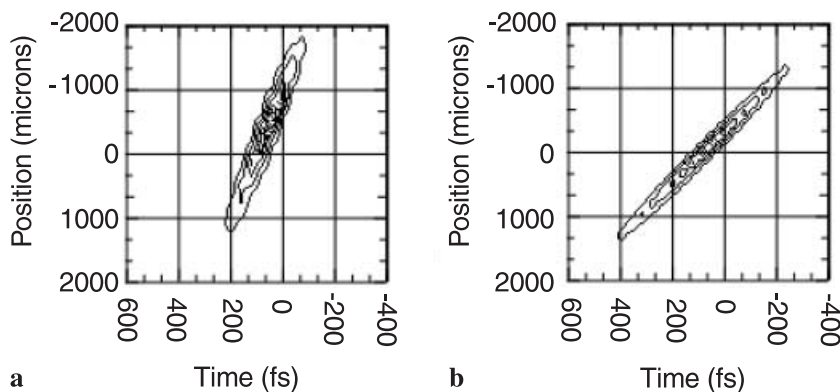

FIGURE 5 Contour plot of the intensity of the field after a Brewster-cut prism (**a**) and a SF10 prism (**b**). The energy of the pulse lies along a straight line $t = \gamma x$ in the (x, t) space

values of γ deduced from these measurements are respectively 91.5 fs mm^{-1} and 241.8 fs mm^{-1}, in good agreement with the calculated values of 90.8 fs mm^{-1} and 247.3 fs mm^{-1} at 815 nm, obtained from the Schott coefficients of these materials.

This space-time coupling is also present in the field after a misaligned compressor. It can be detected by measuring the electric field in the (x, ω) and (y, ω) domains. Although these two measurements do not provide a complete measurement of the field in the (x, y, ω) domain, they are sufficient to track angular dispersion in the electric field. Indeed, angular dispersion of magnitude γ along a direction $\cos(\alpha)x + \sin(\alpha)y$, where α is the angle describing the direction of the angular dispersion relative to the beam wavevector, can be tracked by measuring $\gamma \cos(\alpha)$ along direction x and $\gamma \sin(\alpha)$ along direction y. It is also clear that measurements along both x and y direction are both necessary and sufficient to characterize the spatial chirp in cases where the direction of the dispersion is perpendicular to the direction of measurement. For example, if one measures the field in the (x, ω) space while the dispersion is along y, no information on the dispersion is obtained. A rotation of the input beam by 90° is all that is needed to switch from the first measurement to the second measurement. For a misaligned compressor, our initial measurements of the field gave $\gamma_x = 14$ fs mm^{-1} and $\gamma_y = 63$ fs mm^{-1}, where x lies in an horizontal plane while y lies in a vertical plane. Adjustment of the parallelism of the grooves of the two gratings significantly reduced the angular dispersion in the y direction to a value of $\gamma_y = -0.5$ fs mm^{-1}. Adjustment of the parallelism of the gratings then reduced the angular dispersion in the x direction to a value of $\gamma_x = 0.7$ fs mm^{-1}. A slight astigmatism on the beam was diagnosed, and was attributed to some tilted lenses in the chirped-pulse amplification system. To demonstrate the significance of this optimization, we have plotted in Fig. 6 the ensemble of points in the (x, y, t) domain where the intensity is larger than half the peak intensity before and after optimization. Such a plot clearly emphasizes the space–time localization of the energy of the pulse after optimization. Also, the projections on the (x, t) and (y, t) planes (which are identical to the plot in Fig. 5) show that the pulse is much longer overall than at any particular point across the beam profile before optimization. This information would not be available by conventional (i.e. non-spatially resolved) pulse-characterization techniques.

Space–time coupling may also arise during non-linear propagation and interaction. For example, in birefringent phase-matched non-linear interactions, satisfaction of the phase matching condition depends upon the angles of propagation of the interacting fields in the non-linear medium. Consequently, tightly focused pulses can give rise to a pulse with a spatially dependent frequency content. Although in certain cases this might be useful as a spectrometer [48, 49], it is more usually a condition that one wishes to avoid. Another situation where space–time coupling from non-linear effects occurs is in self-phase modulation. Under intense illumination, the optical index of refraction of light follows the law $n(x, t) = n_0 + n_2 I(x, t)$. For a Gaussian-shaped beam, such propagation induces a non-uniform phase in the spatio-temporal domain. For a positive non-linear index n_2, the field undergoes self-focusing, i.e. the creation of a convergent spatial wavefront, and temporal self-phase modulation. This effect is very detrimental in engineering high-energy lasers, where the B-integral (the integral of the non-linear phase along the propagation path of the beam in the laser system) must be kept below a certain limit in order to get a well-behaved output pulse and not to damage any element in the system. Propagation of our pulses in a 1.25-cm-thick block of SF59 gives rise to a combination of these effects and spectral dispersion. In Fig. 7a, we have plotted the spatio-spectral phase of the output pulse for an energy in the block equal to 42 μJ. Although the input field has nearly zero variation in both the spatial and spectral phases and exhibits no space–time coupling, the output field exhibits focusing, spectral chirp and spatially dependent self-phase modulation which results in strong space–time coupling. In Fig. 7b, we compare the spatial phase of the output field at $t = 0$ for both low-energy and high-energy input fields. As expected, the high-energy field acquires a large bell-shaped spatial phase that follows the spatial intensity at $t = 0$. We point out that in these experimental conditions, the field does not acquire a significant wavefront distortion due to propa-

a   **b**
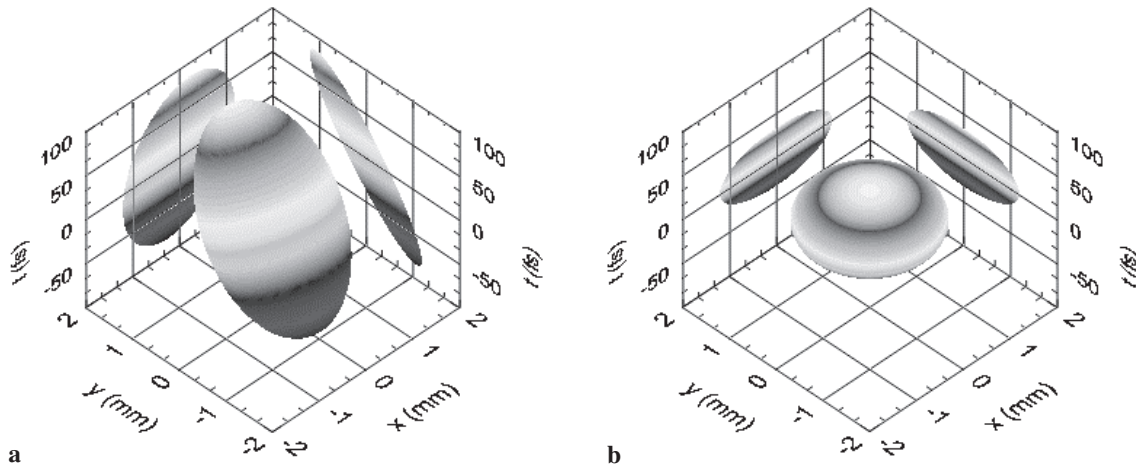
FIGURE 6   Ensemble of points in the (x, y, t) space where the intensity is larger than half the peak intensity of the pulse before (**a**) and after optimization (**b**). The volume of this ensemble is much smaller in the second case, which shows a concentration of the energy of the pulse. The projections on the (x, t) and (y, t) planes (equivalent to the plots of Fig. 5) show significant space–time coupling before optimization
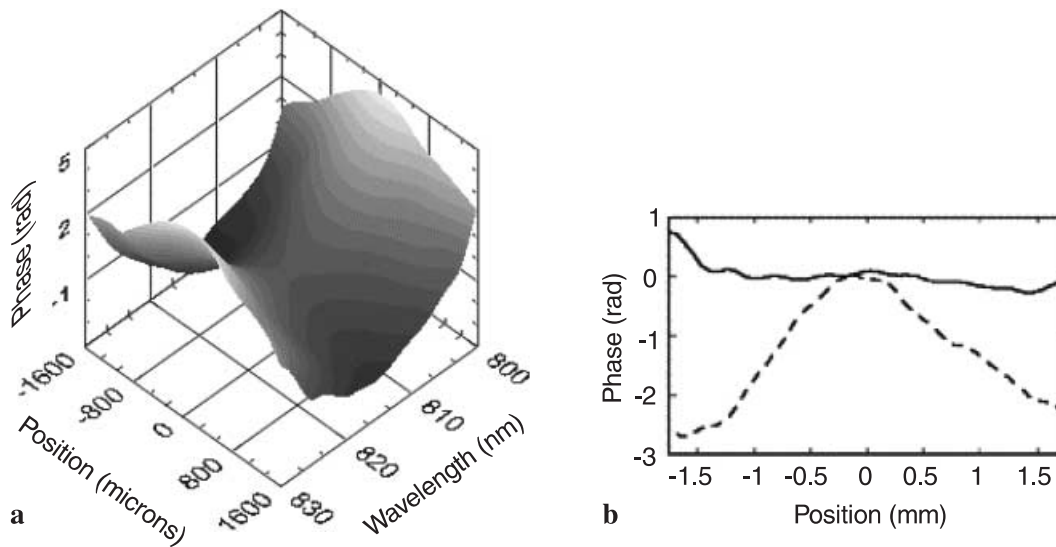
FIGURE 7 Spatio-spectral phase of the electric field after non-linear propagation in a 1.65-cm-thick SF59 block (**a**), and spatial phase at $t = 0$ at low energy and high energy (**b**)

gation in the block since its Rayleigh length is very long. Therefore, we measure a change in the spatial phase but no significant change in the spatial size of the beam. The linear dispersion was found to be 2930 fs^2, in good agreement with the calculated value of 2850 fs^2 at 815 nm for SF59. The non-linear index deduced from this measurement was 6×10^{-15} W^{-1}cm^2, in good agreement with the value of 6.8×10^{-15} W^{-1}cm^2, obtained at a wavelength of 1 μm [50]. The dispersion of the material reduced the peak intensity during propagation of the pulse through the block. Our rough estimate of the non-linear index assumes that the peak intensity in the time and space domains is only modified by the linear properties of the medium during propagation. More accurate results can therefore be expected using a thinner piece of non-linear material, in which case the spatio-temporal phase of the output pulse would be directly proportional to the spatio-temporal intensity.

5   Conclusion

The electric field of light as a function of frequency and space has been measured for the first time to our knowledge using a self-referencing technique. The technique, which extends the principle of two-dimensional shearing interferometry to the (x, ω) domain, allows the direct measurement of two orthogonal gradients of the phase with minimal complexity, and the collection of a modest amount of data and simple signal processing. These two gradients can be coupled to reconstruct the phase, which can be combined with the intensity to yield the complete description of the field. Several experimental demonstrations have been presented showing the power and accuracy of this method.

The method works very well as a beam diagnostic for ultrashort pulse laser systems. We have shown, for example, that it provides a quick and efficient way to precisely align a grating compressor. We expect the technique will also be an invaluable diagnostic for experiments involving ultrashort optical pulses, as well as for other aspects of ultrafast technology in general. The method is easily translatable to other wavelengths.

REFERENCES

1 I. Walmsley, V. Wong: J. Opt. Soc. Am. B **13**, 2453 (1996)
2 E.B. Treacy: J. App. Phys. **42**, 3848 (1971)
3 J. Chilla, O. Martinez: IEEE J. Quantum Electron. **QE-27**, 1228 (1991)
4 R. Trebino, K.W. Delong, D.N. Fittinghoff, J.N. Sweetser, M.A. Krumbugel, B.A. Richman, D.J. Kane: Rev. Sci. Instrum. **68**, 3277 (1997)
5 J. Rhee, T. Sosnowski, A. Tien, T. Norris: J. Opt. Soc. Am. B **13**, 1780 (1996)
6 V. Wong, I. Walmsley: J. Opt. Soc. Am. B **14**, 944 (1997)
7 D.T. Reid: IEEE J. Quantum Electron. **QE-35**, 1584 (1999)
8 R.G.M.P. Koumans, A. Yariv: IEEE J. Quantum Electron. **QE-36**, 137 (2000)
9 J.P. Gex, C. Sauteret, P. Vallat, H. Tourbez, M. Schelev: Opt. Commun. **23**, 430 (1977)
10 K.C. Chu, J.P. Heritage, R.S. Grant, K.X. Liu, A. Dienes, W.E. White, A. Sullivan: Opt. Lett. **20**, 904 (1995)
11 C. Iaconis, I.A. Walmsley: Opt. Lett. **23**, 792 (1998)
12 J. Debeau, B. Kowalski, R. Boittin: Opt. Lett. **23**, 1784 (1998)
13 K. Naganuma, S. Ishibashi: Ultrafast Phenomena **MF7**, (2000)
14 M. Beck, M. Raymer, I. Walmsley, V. Wong: Opt. Lett. **18**, 2041 (1993)
15 M. Kaufman, W. Banyai, A. Godil, D. Bloom: Appl. Phys. Lett. **64**, 270 (1994)
16 H. Lange, M. Franco, J.F. Ripoche, B. Prade, P. Rousseau, A. Mysyrowicz: IEEE J. Sel. Topics Quantum Electron. **4**, 295 (1998)
17 C.V. Bennett, B.H. Kolner: Opt. Lett. **24**, 783 (1999)
18 C. Yan, J.C. Diels: J. Opt. Soc. Am. B **8**, 1259 (1991)
19 A. Baltuska, A. Pugzlys, M. Pshenichnikov, D.A. Wiersma: 'Rapid Amplitude-Phase Reconstruction of Femtosecond Pulses from Intensity Autocorrelation and Spectrum'. In: Conf. on Lasers, Electro-Optics, 1999 OSA Technical Digest Series, 264 (1999)
20 K. Naganuma, K. Mogi, H. Yamada: IEEE J. Quantum Electron. **QE-25**, 1225 (1989)
21 J.W. Nicholson, J. Jasapara, W. Rudolph, F.G. Omenetto, A.J. Taylor: Opt. Lett. **24**, 1774 (1999)
22 Z. Bor: Opt. Lett. **14**, 119 (1989)
23 M.M. Wefers, K.A. Nelson: IEEE J. Quantum Electron. **QE-32**, 161 (1996)
24 C. Fiorini, S. Sauteret, C. Rouyer, N. Blanchot, S. Seznec, A. Migus: IEEE J. Quantum Electron. **QE-30**, 1662 (1994)
25 M.M. Wefers, K.A. Nelson, A.M. Weiner: Opt. Lett. **21**, 746 (1996)
26 J.C. Chanteloup, E. Salmon, C. Sauteret, A. Migus, P. Zeitoun, A. Klisnick, A. Carillon, S. Hubert, D. Ros, P. Nickles, M. Kalachnikov: JOSA B – Opt. Phys. **17**, 151 (2000)
27 B.A. Richman, S.E. Bisson, R. Trebino, E. Sidick, A. Jacobson: Appl. Opt. **38**, 3316 (1999)
28 M. Françon: *Optical Interferometry* (Academic Press, New York, London 1966)
29 D. Malacara: *Optical Shop Testing*, 2nd edn. (Wiley, New York 1992)

30 L. Gallmann, D.H. Sutter, N. Matuschek, G. Steinmeyer, U. Keller, C. Iaconis, I.A. Walmsley: Opt. Lett. **24**, 1314 (1999)
31 C. Dorrer, B. de Beauvoir, C. Le Blanc, S. Ranc, J.P. Rousseau, P. Rousseau, J.P. Chambaret: Opt. Lett. **24**, 1644 (1999)
32 S. Rivet, L. Canioni, R. Barille, L. Sarger: Ultrafast Optics **M 20**, (2001)
33 S.A. Diddams, H.K. Eaton, A.A. Zozulya, T.S. Clement: Conference on Lasers and Electro-Optics (CLEO/US), Vol. 6 of 1998 OSA Technical Digest Series (Optical Society of Amaerica, Washington DC, 1998), paper CFF3
34 R.N. Smartt, W.H. Steel: SPIE Milestone Series **28**, 272 (1991)
35 L. Gallmann, G. Steinmeyer, D.H. Sutter, T. Rupp, C. Iaconis, I.A. Walmsley, U. Keller: Opt. Lett. **26**, 96 (2001)
36 Z. Sacks, G. Mourou, R. Danielius: Opt. Lett. **26**, 462 (2001)
37 C. Froehly, A. Lacourt, C. Viénot: Nouv. Rev. Optique **4**, 183 (1973)
38 L. Lepetit, G. Cheriaux, M. Joffre: JOSA B – Opt. Phys. **12**, 2467 (1995)
39 Z. Bor, Z. Gogolak, G. Szabo: Opt. Lett. **14**, 862 (1989)
40 C. Radzewicz, M.J. la Grone, J.S. Krasinski: Opt. Commun. **126**, 185 (1996)
41 J. Jasapara, W. Rudolph: Opt. Lett. **24**, 777 (1999)
42 R. Netz, T. Feurer, R. Wolleschensky, R. Sauerbrey: App. Phys. B – Lasers, Optics **70**, 833 (2000)
43 M. Murty: 'Lateral Shearing Interferometers'. In: *Optical Shop Testing*, ed. by D. Malacara (Wiley, New York 1978) pp. 117–118
44 C. Dorrer: JOSA B – Opt. Phys. **16**, 1160 (1999)
45 C. Dorrer: Opt. Lett. **24**, 1532 (1999)
46 I. Walmsley, L. Waxer, C. Dorrer: Rev. Sci. Instrum. **72**, 1 (2001)
47 Z. Bor, B. Racz, G. Szabo, M. Hilbert, H.A. Hazim: Opt. Eng. **32**, 2501 (1993)
48 C. Radzewicz, P. Wasylczyk, J.S. Krasinski: Opt. Commun. **186**, 329 (2000)
49 P. O'Shea, P. Kimmel, X. Gu, R. Trebino: Opt. Lett. **26**, 932 (2001)
50 S.R. Friberg, S.W. Smith IEEE J. Quantum Electron. **QE-23**, 2089 (2001)